Article

Brightest Point in Accretion Disk and Black Hole Spin: Implication to the Image of Black Hole M87*

Vyacheslav I. Dokuchaev [1,2]* and Natalia O. Nazarova [3]

[1]   Institute for Nuclear Research of the Russian Academy of Sciences, Moscow, 117312 Russia
[2]   Moscow Institute of Physics and Technology, 9 Institutskiy per., Dolgoprudny, Moscow Region, 141700 Russia
[3]   Scuola Internazionale Superiore di Studi Avanzati (SISSA), Via Bonomea 265, 34136 Trieste (TS) Italy; natalia.nazarova@sissa.it
*   Correspondence: dokuchaev@inr.ac.ru

Abstract: A dark region and a bright part of accretion disk are viewed on the first image of the supermassive black hole in the galaxy M87 obtained by the Event Horizon Telescope. We demonstrate that a viewed dark region is a silhouette of the black hole event horizon, while the outline (contour) of this silhouette is an equator of the event horizon globe. A dark silhouette of the black hole event horizon is placed within the expected position of the black hole shadow, which is not revealed on the first image. We calculate numerically a relation between the viewed position of the black hole silhouette and the brightest point in a thin accretion disk in dependence of the black hole spin. A spin of the supermassive black hole in the galaxy M87, derived from this relation, is $a = 0.75 \pm 0.15$.

Keywords: General Relativity, gravity, black hole, black hole shadow

PACS: 04.70.Bw, 98.35.Jk, 98.62.Js

---

1. Introduction

The Event Horizon Telescope (EHT) recently presented for the first time an impressive image of the supermassive black hole in the galaxy M87 [1–6]. There are two specific features on this image: the dark silhouette and the bright region.

A rather obviously to suppose that the bright region is related with the emission of accreting matter around the supermassive black hole M87*. But what is a physical origin of the dark silhouette, viewed on the presented image? It depends on the black hole astrophysical environment.

A black hole shadow is viewed by a distant observer in the case of a stationary luminous background, placed beyond the unstable circular photon orbit $r_{\rm ph}$ [7–22]. In the pioneering work of J. M. Bardeen [7] a black hole shadow was called the "apparent boundary" of the black hole.

The quite different case is a black hole image produced by the luminous non-stationary matter plunging into black hole in a region between the unstable circular photon orbit $r_{\rm ph}$ and the black hole event horizon $r_{\rm ph}$. An evident example of the luminous non-stationary matter is the inner region of thin accretion disk between the Innermost Stable Circular Orbit $r_{\rm ISCO}$ (see definition, e. g., in[23]) and the event horizon. A non-stationary luminous matter in this region is spiraling down toward the event horizon and produces a dark image of the event horizon silhouette instead of the black hole shadow [8,25–32]. In addition, the outline (contour) of this silhouette is an image of the event horizon equator [33–35].

In this paper we calculate numerically a form of the event horizon silhouette of the rotating Kerr black hole by modeling the emission of non-stationary luminous matter spiraling down into black hole in the inner region of thin accretion disk at $r_{\rm ISCO} \leq r \leq r_{\rm h}$. The trajectories of photons are calculated in the geometric optic approximation and it is also supposed that accretion disk is optically thin. The

event horizon silhouette is smaller than the black hole shadow and is placed on the celestial sphere within the awaited position of black hole shadow.

We identify the dark region on the EHT image with the event horizon silhouette and, respectively, the bright region with the brightest point in accretion disk. For a case of the supermassive black hole M87* we find a distance of the brightest point in the thin accretion disk from the center of event horizon silhouette in dependence of the black hole spin parameter a. In result, from this dependence we find that a spin of the supermassive black hole M87* is $a = 0.75 \pm 0.15$.

2. Photon trajectories in Kerr metric

We describe the trajectories of photons (null geodesics) in Kerr metric by using the standard Boyer–Lindquist coordinate system [36] with coordinates (t, r, θ, φ) and with units $G = c = 1$. Additionally we put $mG/c^2 = 1$. With these units a dimensionless radius of the black hole event horizon is $r_{\rm h} = 1 + \sqrt{1 - a^2}$, where a spin parameter of the black hole $0 \leq a \leq 1$.

Trajectories of particles with a rest mass μ in the Kerr space-time are determined by three constants of motion: a total energy E, a component of angular momentum parallel to symmetry axis (azimuth angular momentum) L and the Carter constant Q, which is related with the non-equatorial motion of particles [9,37]. Particle trajectories (geodesics) in the radial and latitudinal directions are defined, correspondingly, by a radial effective potential

$$R(r) = [E(r^2 + a^2) - La]^2 - (r^2 - 2r + a^2)[\mu^2 r^2 + (L - aE)^2 + Q] \tag{1}$$

and a latitudinal effective potential

$$\Theta(\theta) = Q - \cos^2\theta[a^2(\mu^2 - E^2) + L^2/\sin^2\theta]. \tag{2}$$

Trajectories of photons (null geodesics with $\mu = 0$) in the Kerr space-time are determined only by two dimensionless parameters, $\lambda = L/E$ and $q^2 = Q/E^2$. These parameters are related with the impact parameters on the celestial sphere α and β seen by a distant observer placed at a given radius $r_0 \gg r_{\rm h}$ (i.e., practically at infinity), at a given latitude θ_0 and at a given azimuth φ_0 (see, e.g., [7,38] for more details):

$$\alpha = -\frac{\lambda}{\sin\theta_0}, \quad \beta = \pm\sqrt{\Theta(\theta_0)}, \tag{3}$$

where $\Theta(\theta)$ is from (2).

We use integral equations of motion for photons [9,37] for numerical calculations of the gravitational lensing by the Kerr black hole

$$\fint^r \frac{dr}{\sqrt{R(r)}} = \fint^\theta \frac{d\theta}{\sqrt{\Theta(\theta)}}, \tag{4}$$

$$\varphi = \fint^r \frac{a(r^2 + a^2 - \lambda a)}{(r^2 - 2r + a^2)\sqrt{R(r)}} dr + \fint^\theta \frac{\lambda - a\sin^2\theta}{\sin^2\theta\sqrt{\Theta(\theta)}} d\theta, \tag{5}$$

$$t = \fint^r \frac{(r^2 + a^2)P}{(r^2 - 2r + a^2)\sqrt{R(r)}} dr + \fint^\theta \frac{(L - aE\sin^2\theta)a}{\sqrt{\Theta(\theta)}} d\theta, \tag{6}$$

where the effective potentials V_r and $V_\backprime$ are from Eqs. (17) and (2). The integrals in (4), and (5) are understood to be path integrals along the trajectory.

The path integrals in (4), (5) and (6) are the ordinary ones for photon trajectories without the turning points:

$$\int_{r_s}^{r_0} \frac{dr}{\sqrt{R(r)}} = \int_{\theta_s}^{\theta_0} \frac{d\theta}{\sqrt{\Theta(\theta)}}. \tag{7}$$
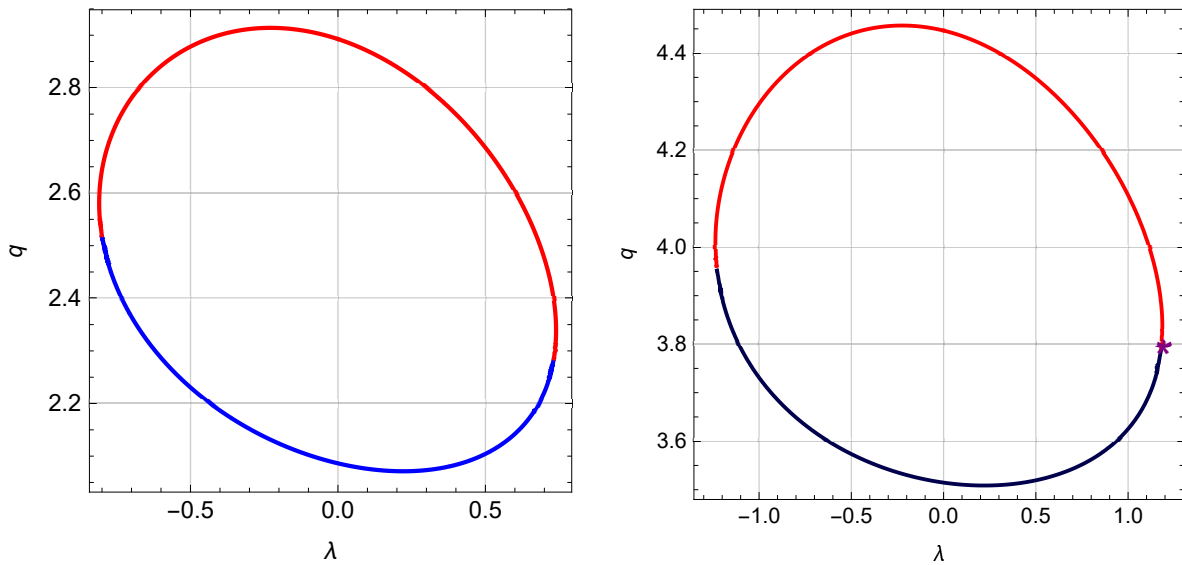
Figure 1. Parameters of photon trajectories λ and q, reaching a distant observer from the rings in accretion disk at $r = 0.01r_{\mathrm{h}}$ (left graph) and at $r = r_{\mathrm{ISCO}}$ (right graph). It is shown the case of rotating black hole with spin $a = 0.75$ in the galaxy M87, corresponding to $\theta_0 = 17°$. The blue color corresponds to photon trajectories without the turning points, defined from numerical solutions of integral equation (7). The red color corresponds to photon trajectories with only one turning point at $\theta = \theta_{\min}(\lambda, q)$, defined from numerical solutions of integral equation (8). The brightest point (marked by a star "★") in accretion disk is placed at radius $r_{\mathrm{ISCO}} \simeq 1.16r_{\mathrm{h}}$ and corresponds to the photon trajectory without turning points and with the maximum permissible azimuth angular momentum. Parameters of photon trajectory from the brightest point are $\lambda = 1.18$ and $q = 3.79$ or $\alpha = -4.03$ and $\beta = -0.18$.

In the case of photon trajectories with one turning point $\theta_{\min}(\lambda, q)$ (an extremum of latitudinal potential $\Theta(\theta)$), equation (4) is written through the ordinary integrals as

$$\int_{r_s}^{r_0} \frac{dr}{\sqrt{R(r)}} = \int_{\theta_{\min}}^{\theta_s} \frac{d\theta}{\sqrt{\Theta(\theta)}} + \int_{\theta_{\min}}^{\theta_0} \frac{d\theta}{\sqrt{\Theta(\theta)}}. \tag{8}$$

In general, a lensed black hole produces infinite number of images [38–41]. Except the very special orientation cases, the most luminous image is a so called direct or prime image, produced by photons which do not intersect the black hole equatorial plane on the way to a distant observer. Meantime, the secondary images (named also as the higher order images or light echoes), produced by photons which intersect the black hole equatorial plane several times. The energy flux from secondary images as a rule is very small with respect to one from direct image.

3. Black hole shadow

A black hole shadow is the gravitational capture cross-section of photons from the stationary luminous background placed at radial distance from black hole exceeding the radius of unstable photon circular orbit r_{ph} (see definition in [23]) to form the image of black hole shadow.

A black hole shadow in the Kerr metric, projected on the celestial sphere and seen by a distant observer in the equatorial plane of the black hole, is determined from the simultaneous solution of equations $R(r) = 0$ and $[rR(r)]' = 0$, where the effective radial potential $R(r)$ is from Eq. (17). The corresponding solution for the black hole shadow (for a distant observer in the black hole equatorial plane) in the parametric form $(\lambda, q) = (\lambda(r), q(r))$ is

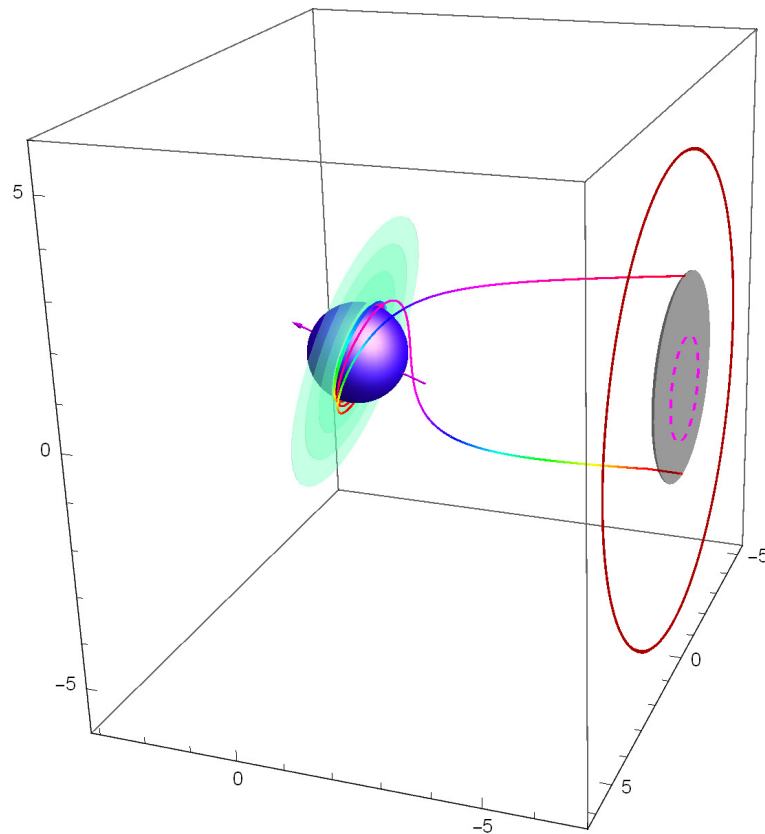$$\lambda = \frac{-r^3 + 3r^2 - a^2(r+1)}{a(r-1)}, \quad q^2 = \frac{r^3[4a^2 - r(r-3)^2]}{a^2(r-1)^2}. \tag{9}$$

Figure 2. Two 3D photon trajectories starting from a thin accretion disk (light green oval) at $r = 1.01 r_{\mathrm{h}}$ in the case of black hole with $a = 0.9982$ and reaching a distant observer very near the outline (contour) of the event horizon silhouette (light black region). In the case of M87* the viewed dark silhouette is a southern hemisphere of the black hole horizon. A closed dark red curve is a border of the black shadow. Parameters of these photon trajectories are $\lambda = -0.047$ and $q = 2.19$ and, respectively, $\lambda = -0.029$, $q = 1.52$. A dashed red circle is a viewed position of the black hole event horizon in the imaginary Euclidian space.

(see, e. g., [7,9] for more details).

Quite a different black hole image produced in the case of black hole highlighted by the non-stationary luminous matter plunging into black hole inside the radius of unstable photon circular orbit r_{ph}.

4. Event horizon silhouette

A viewed dark event horizon silhouette is recovered by gravitational lensing of photons emitted in the innermost part of accretion disk adjoining the event horizon. In a geometrically thin accretion disk, placed in the equatorial plane of the black hole, there is an inner boundary for stable circular motion, named the marginally stable radius or the Inner Stable Circular Orbit (ISCO), $r = r_{\mathrm{ISCO}}$ (see e. g., [23] for more details):

$$r_{\mathrm{ISCO}} = 3 + Z_2 - \sqrt{(3 - Z_1)(3 + Z_1 + 2Z_2)}, \tag{10}$$

where

$$Z_1 = 1 + (1 - a^2)^{1/3}[(1 + a)^{1/3} + (1 - a)^{1/3}], \quad Z_2 = \sqrt{3a^2 + Z_1^2}. \tag{11}$$

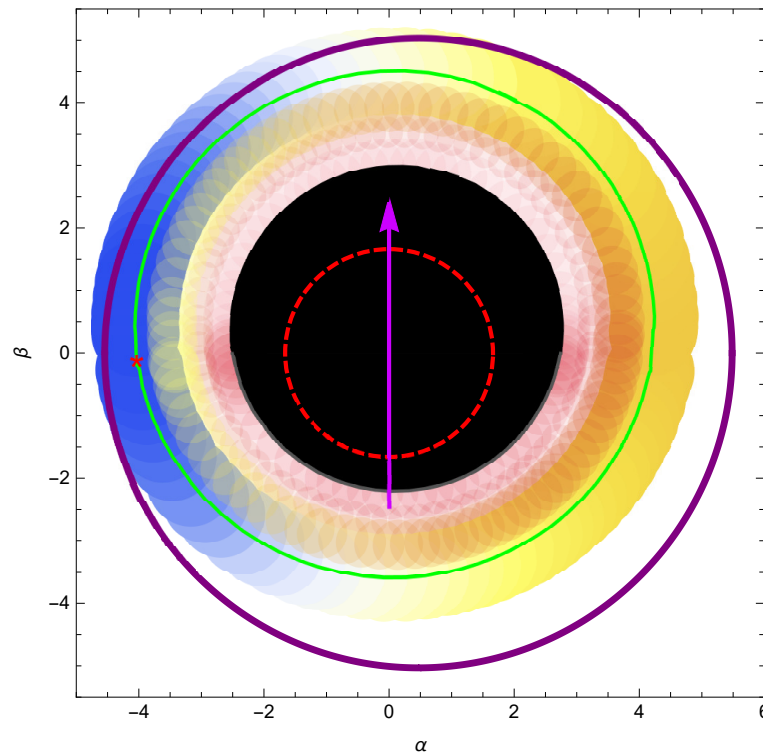**Figure 3.** Internal part of the lensed accretion disk at $r_h \leq r \leq r_{ISCO}$ adjoining the event horizon in a case of non-rotating black hole with spin $a = 0$. The brightest point in accretion disk is at radius $r_{ISCO} = 6 = 3r_h$ and corresponds to the photon trajectory with $\lambda = 6.89$, $q = 0.697$, $\alpha = -6.92$, $\beta = -0.057$.

The corresponding values of parameters E and L for particles in the accretion disk co-rotating with the black hole at a circular orbit with a radius r are obtained from the simultaneous solution of equations $R = 0$ and $dR/dr = 0$, where the effective radial potential R is from (1):

$$\frac{E}{\mu} = \frac{r^{3/2} - 2r^{1/2} + a}{r^{3/4}(r^{3/2} - 3r^{1/2} + 2a)^{1/2}} \tag{12}$$

$$\frac{L}{\mu} = \frac{r^2 - 2ar^{1/2} + a^2}{r^{3/4}(r^{3/2} - 3r^{1/2} + 2a)^{1/2}}. \tag{13}$$

We use a simple model for describing the non-stationary motion of small gas elements of accreting matter in the region at $r_h \leq r \leq r_{ISCO}$ by supposing of a pure geodesic motion of the separate compact gas element (or compact gas clump) in the accretion flow with orbital parameters E and L from (12) and (13), corresponding to the radius $r = r_{ISCO}$. We suppose also that a thin accretion disk is transparent and the energy flux in the rest frame of small gas elements is isotropic and conserved during their spiraling down into the black hole.

See in Figure 1 parameters of photon trajectories λ and q, reaching a distant observer from the rings in accretion disk at $r = 0.01r_h$ and at $r = r_{ISCO}$. It is shown the case of rotating black hole with spin $a = 0.75$ in the galaxy M87, corresponding to $\theta_0 = 17°$.

To calculate the energy shift of photons and energy flux from the lensed image of accretion disk it is needed to take into account both a red-shift in the black hole gravitational field and Doppler effect. It is convenient to use in this calculations the orthonormal Locally Non-Rotating Frames (LNRF) [23,24], for which the observers' world lines are $r = const$, $\theta = const$, $\varphi = \omega t + const$, where a frame dragging angular velocity

$$\omega = \frac{2ar}{(r^2 + a^2)^2 - a^2(r^2 - 2r + a^2)\sin^2\theta}. \tag{14}$$
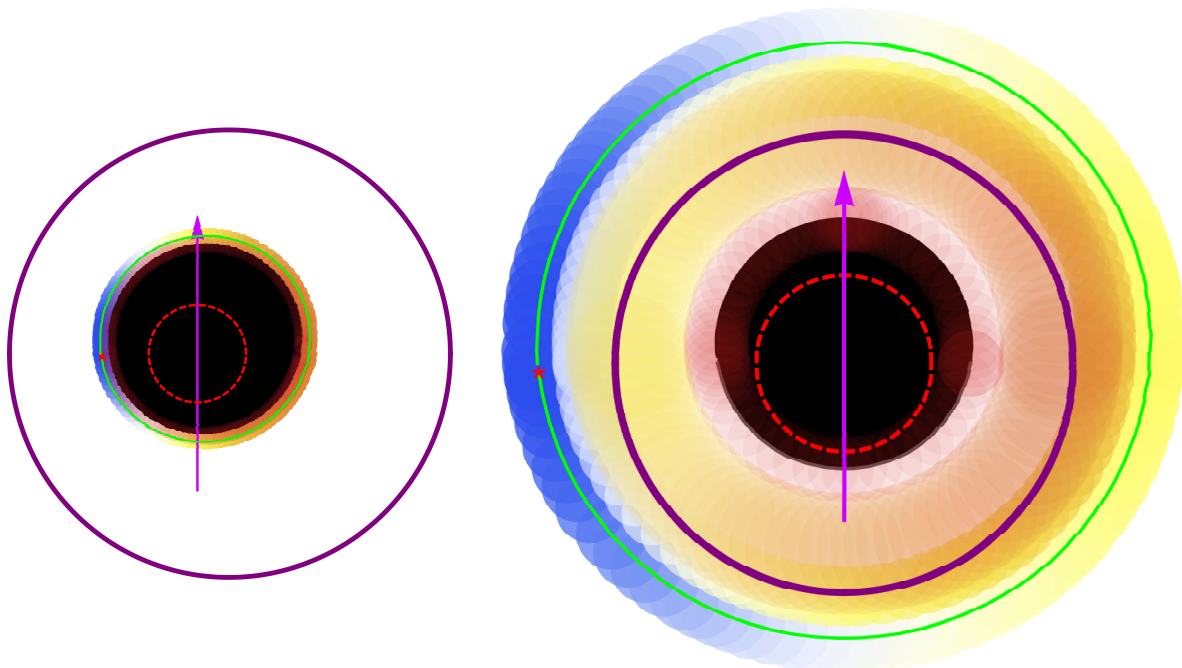
Figure 4. Silhouette of the southern hemisphere of the black hole event horizon (black region) projected inside the black hole shadow (closed purple curves) for black hole in the galaxy M87, $\theta_0 = 17°$. Positions of the brightest points in accretion disk are marked by red stars ★ in the case of black hole spin $a = 0.9882$ (left image) and $a = 0$ (right image), respectively.

The requested photon energy in the frame, comoving with the compact gas cloud at $\theta = \pi/2$, is [35,39]

$$\mathcal{E}(\lambda, q) = \frac{P^{(t)} - V^{(\varphi)}p^{(\varphi)} - V^{(r)}p^{(r)}}{\sqrt{1 - [V^{(r)}]^2 - [V^{(\varphi)}]^2}}. \tag{15}$$

In this equation the azimuth velocity $V^{(\varphi)}$ of a compact gas cloud with orbital parameters E, L and $Q = 0$ relative the LNRF, falling in the equatorial plane onto a black hole, is

$$V^{(\varphi)} = \frac{r\sqrt{r^2 - 2r + a^2}\, L}{[r^3 + a^2(r+2)]E - 2aL}. \tag{16}$$

A corresponding radial velocity in the equatorial plane relative the LNRF is

$$V^{(r)} = -\sqrt{\frac{r^3 + a^2(r+2)}{r}}\, \frac{\sqrt{R(r)}}{[r^3 + a^2(r+2)]E - 2aL}. \tag{17}$$

where $R(r)$ is defined in (1) with $Q = 0$. The components of photon 4-momentum in the LNRF are

$$p^{(\varphi)} = \sqrt{\frac{r}{r^3 + a^2(r+2)}}\, \lambda, \quad p^{(t)} = \sqrt{\frac{r^3 + a^2(r+2)}{r(r^2 - 2r + a^2)}}\, (1 - \omega\lambda), \tag{18}$$

$$p^{(r)} = -\frac{1}{r}\sqrt{\frac{(r^2 + a^2 - a\lambda)^2}{r^2 - 2r + a^2} - [(a - \lambda)^2 + q^2]}. \tag{19}$$

Respectively, the energy shift (the ratio of photon frequency at infinity to a corresponding one in the rest frame of the compact gas clump) is $g(\lambda, q) = 1/\mathcal{E}(\lambda, q)$. This energy shift is used in numerical
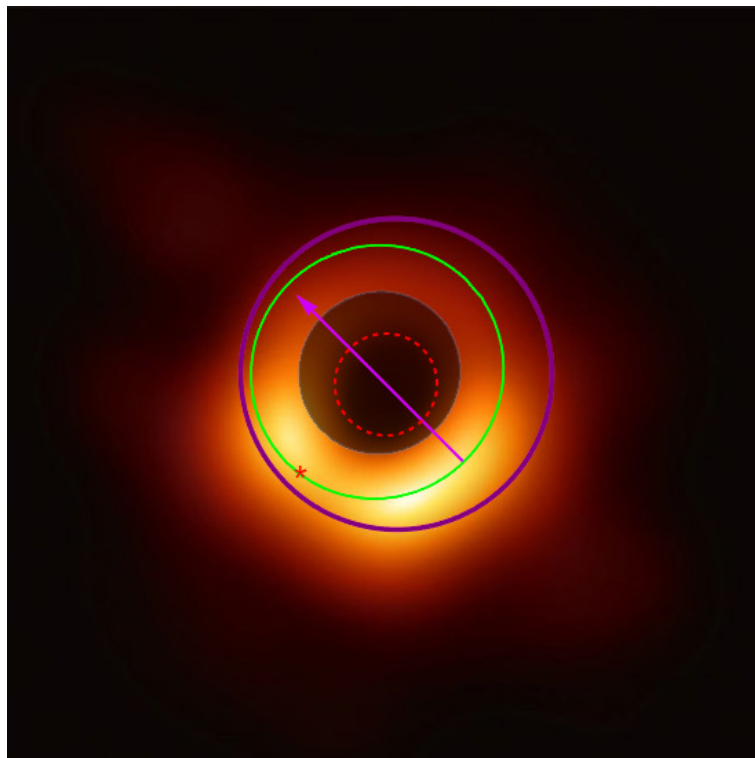
Figure 5. Superposition of the M87* image, obtained by EHT [1–6], and the thin disk model from Figure 3 in the case of $a = 0.75$. Star ⋆ here and as well as in all other similar Figures. marks the viewed position of the brightest point in the thin accretion disk.

calculations of the energy flux from the accretion disk elements measured by a distant observer, following formalism by C. T. Cunnungham and J. M. Bardeen [38].

5. Spin of the black hole M87*

Model direct images of the inner non-stationary part of thin accretion disk in the region $r_{\rm rh} \leq r \leq r_{\rm ISCO}$, adjoining the black hole event horizon, are presented in Figures 2–5. The gravitational red-shift and Doppler effect are taken into account in these images. Local artificial colors of the thin accretion disk images are related with an effective local black-body temperature of the accreting gas elements. These numerical calculations demonstrate that a viewed brightest point in the thin accretion disk is always (for all values of black hole spin a) placed at radius $r = r_{\rm ISCO}$ at the point corresponding to photon trajectory without turning point and with the maximum permissible azimuth angular momentum $\lambda > 0$.

The derived relation between position of the brightest point in the thin accretion disk and the viewed black hole silhouette in dependence of the black hole spin is shown in Figure 5. From comparison of this relation with the image obtained by EHT it is followed that spin of the supermassive black hole of M87* is $a = 0.75 \pm 0.15/$. See in Figure 6 the superposition of M87* image and the modeled image of thin accretion disk in the case of $a = 0.65$.

6. Conclusions

We calculated numerically a form of the event horizon silhouette of the rotating Kerr black hole by modeling the emission of non-stationary luminous matter spiraling down into the black hole in the inner region of thin accretion disk at $r_{\rm ISCO} \leq r \leq r_{\rm h}$. The resulting form of the event horizon silhouette does not depend on the local emission of accretion disk and governed completely by the gravitational field of the black hole. In a case of the supermassive black hole M87*, viewed at the inclination angle
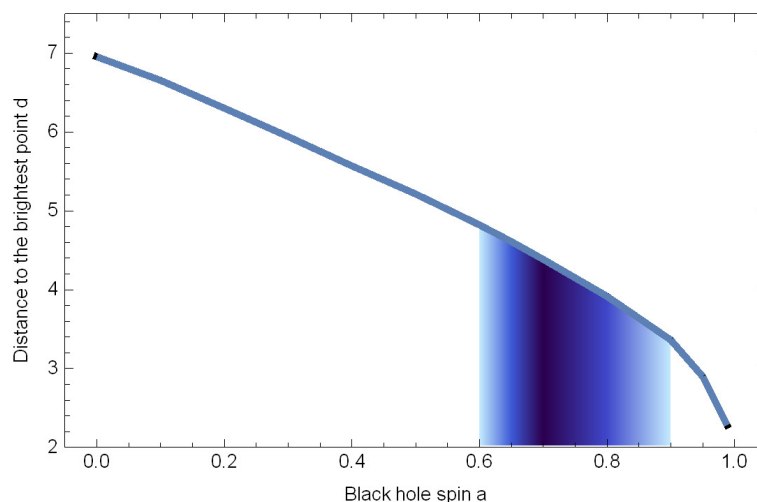
Figure 6. Relation between a distance $d(a)$ of the brightest point in accretion disk from the center of viewed black hole silhouette in dependence of the black hole spin a for the case of M87*.

$17°$, a dark silhouette on the EHT image is the southern hemisphere of the black hole event horizon. The contour of this silhouette is an equator of the event horizon.

The brightest point in accretion disk corresponds to the largest (positive) azimuth angular momentum λ of photon with the direct orbit, reaching a distant observer without the turning points. By using the first image of the black hole in the galaxy M87, obtained by the EHT, we find that the corresponding value of the black hole spin is $a = 0.75 \pm 0.15$.

Author Contributions: Authors contributed to the paper equally.

Conflicts of Interest: The authors declare no conflict of interest.

Abbreviations

The following abbreviations are used in this manuscript:

EHT   Event Horizon Telescope
LNRF   Locally Non-Rotating Frames

References

1. Event Horizon Telescope Collaboration, K. Akiyama, Alberdi, A.; Alef, W.; Asada, K.; Azulay, R.; Baczko, A.-K.; Ball, D.; Balokovic, M.; Barrett, J.; et al. M87 Event Horizon Telescope Results. I. The Shadow of the Supermassive Black Hole. *Astrophys. J.* **2019**, *875*, L1; DOI: 10.3847/2041-8213/ab0ec7.
2. Event Horizon Telescope Collaboration, K. Akiyama, Alberdi, A.; Alef, W.; Asada, K.; Azulay, R.; Baczko, A.-K.; Ball, D.; Balokovic, M.; Barrett, J.; et al. M87 Event Horizon Telescope Results. II. Array and Instrumentation. *Astrophys. J.* **2019**, *875*, L2; DOI: 10.3847/2041-8213/ab0c96.
3. Event Horizon Telescope Collaboration, K. Akiyama, Alberdi, A.; Alef, W.; Asada, K.; Azulay, R.; Baczko, A.-K.; Ball, D.; Balokovic, M.; Barrett, J.; et al. M87 Event Horizon Telescope Results. III. Data Processing and Calibration. *Astrophys. J.* **2019**, *875*, L3; DOI: 10.3847/2041-8213/ab0c57.
4. Event Horizon Telescope Collaboration, K. Akiyama, Alberdi, A.; Alef, W.; Asada, K.; Azulay, R.; Baczko, A.-K.; Ball, D.; Balokovic, M.; Barrett, J.; et al. M87 Event Horizon Telescope Results. IV. Imaging the Central Supermassive Black Hole. *Astrophys. J.* **2019**, *875*, L4; DOI: 10.3847/2041-8213/ab0e85.

5.   Event Horizon Telescope Collaboration, K. Akiyama, Alberdi, A.; Alef, W.; Asada, K.; Azulay, R.; Baczko, A.-K.; Ball, D.; Balokovic, M.; Barrett, J.; et al. M87 Event Horizon Telescope Results. V. Physical Origin of the Asymmetric Ring. *Astrophys. J.* **2019**, *875*, L5; DOI: 10.3847/2041-8213/ab0f43.

6.   Event Horizon Telescope Collaboration, K. Akiyama, Alberdi, A.; Alef, W.; Asada, K.; Azulay, R.; Baczko, A.-K.; Ball, D.; Balokovic, M.; Barrett, J.; et al. M87 Event Horizon Telescope Results. VI. The Shadow and Mass of the Central Black Hole. *Astrophys. J.* **2019**, *875*, L6; DOI: 10.3847/2041-8213/ab1141.

7.   Bardeen J.M. Timeline and Null Geodesics in the Kerr Metric. In *Black Holes*; DeWitt, C., DeWitt B.S., Eds.; Gordon and Breach, New York, 1973; p. 217–239.

8.   Luminet J.-P. Image of a spherical black hole with thin accretion disk. *Astron. Astrophys.* **1979**, *75*, 228–235.

9.   Chandrasekhar S. *The Mathematical Theory of Black Holes*; Clarendon Press: Oxford, UK, 1983.

10. Falcke, H.; Melia, F.; Agol, E. Viewing the Shadow of the Black Hole at the Galactic Center. *Astrophys. J.* **2000**, *528*, L13–L16; DOI: 10.1086/312423.

11. Zakharov, A.F.; De Paolis, F.; Ingrosso G.; Nucita, A.A. Measuring the black hole parameters in the galactic center with RADIOASTRON. *New Astron.* **2005**, *10*, 479-489; DOI: 10.1016/j.newast.2005.02.007.

12. Johannsen T.; Psaltis, D. Testing the No-hair Theorem with Observations in the Electromagnetic Spectrum. II. Black Hole Images. *Astrophys. J.* **2010**, *718*, 446–454; DOI: 10.1088/0004-637X/718/1/446.

13. Grenzebach, A.; Perlick, V.; Lämmerzahl. C. Photon regions and shadows of Kerr-Newman-NUT black holes with a cosmological constant. *Phys. Rev. D* **2014**, *89*, 124004; DOI: 10.1103/PhysRevD.89.124004.

14. Grenzebach, A.; Perlick, V.; Lämmerzahl. Photon regions and shadows of accelerated black holes. *Int. J. Mod. Phys. D* **2015**, *24*, 1542024; DOI: 10.1142/S0218271815420249.

15. Cunha, P.V.P.; Herdeiro C.A.R. Shadows and strong gravitational lensing: a brief review. *Gen. Relativ. Gravit.* **2018**, *50*, 42; DOI: 10.1007/s10714-018-2361-9.

16. Cunha, P.V.P.; Herdeiro C.A.R.; Rodriguez M.J. Does the black hole shadow probe the event horizon geometry? *Phys. Rev. D* **2018**, *97*,084020; DOI: 10.1103/PhysRevD.97.084020.

17. Huang, Yang; Dong, Yi-Ping; Liu, Dao-Jun. Revisiting the shadow of a black hole in the presence of a plasma. *Int. J. Mod. Phys. D* **2018**, *27*,1850114; DOI: 10.1103/PhysRevD.97.084020.

18. Gralla, S.E.; Porfyriadis, A.P.; Warburton, N. Particle on the innermost stable circular orbit of a rapidly spinning black hole. **2015**, *92*, 064029; DOI: 10.1103/PhysRevD.92.064029.

19. Gralla, S.E.; Lupsasca, A.; Strominger, A. Near-horizon Kerr magnetosphere. *Phys. Rev. D* **2016**, *93*, 104041; DOI: 10.1103/PhysRevD.93.104041.

20. Gralla, S.E.; Zimmerman, A.; Zimmerman, P. Transient instability of rapidly rotating black holes. *Phys. Rev. D* **2016**, *94*, 084017; DOI: 10.1103/PhysRevD.94.084017.

21. Porfyriadis, A.P.; Shi, Y.; Strominger, A. Photon emission near extreme Kerr black holes. *Phys. Rev. D* **2017**, *95*, 064009; DOI: 10.1103/PhysRevD.95.064009.

22. S. E. Gralla, A. Lupsasca, and A. Strominger. Observational signature of high spin at the Event Horizon Telescope. *Mon. Not. R. Astron. Soc.* **2017**, *475*, 3829–3853; DOI: 10.1093/mnras/sty039.

23. Bardeen, J.M.; Press, W.H.; Teukolsky, S.A. Rotating Black Holes: Locally Nonrotating Frames, Energy Extraction, and Scalar Synchrotron Radiation. *Astrophys. J.* **1972**, *178*, 347–370; DOI: 10.1086/151796.

24. Bardeen J.M. Stability of Circular Orbits in Stationary, Axisymmetric Space-Times. *Astrophys. J.* **1970**, *162*, 103–109; DOI: 10.1086/150515.

25. Dexter, J.; Agol, E.; Fragile, P.C. Millimeter Flares and VLBI Visibilities from Relativistic Simulations of Magnetized Accretion onto the Galactic Center Black Hole. *Astrophys. J.* **2009**, *703*, L142–L146; DOI: 10.1088/0004-637X/703/2/L142.

26. Bromley, B.C.; Chen, K.; Miller, W.A. Line Emission from an Accretion Disk around a Rotating Black Hole: Toward a Measurement of Frame Dragging. *Astrophys. J.* **1997**, *475*, 57–64; DOI: 10.1086/303505.

27. C. Fanton, M. Calvani, F. de Felice, and A. Cadez. Detecting Accretion Disks in Active Galactic Nuclei. *Publ. Astron. Soc. Japan* **1997**, *49*, 159–169; DOI: 10.1093/pasj/49.2.159.

28. Fukue, J. Silhouette of a Dressed Black Hole. *Publ. Astron. Soc. Japan* **2003**, *55*, 155–159; DOI: 10.1093/pasj/55.1.155.

29. J. Fukue. Light-Curve Diagnosis of a Hot Spot for Accretion-Disk Models. *Publ. Astron. Soc. Japan* **2003**, *55*, 1121–1125; DOI: 10.1093/pasj/55.6.1121.

30. Lu, R.; Roelofs, F.; Fish, V.L.; Shiokawa, H.; Doeleman, S.S.; Gammie, C.F.; Falcke, H.; Krichbaum, T.P.; Zensus, J.A. Imaging an Event Horizon: Mitigation of Source Variability of Sagittarius A*. *Astrophys. J.* **2016**, *817*, 173; DOI: 10.3847/0004-637X/817/2/173.

31. Luminet, J..-P. An Illustrated History of Black Hole Imaging : Personal Recollections (1972-2002). *arXiv* **2019**, arXiv:1902.11196 [astro-ph.HE].

32. Shiokawa, H. **2019**, https://eventhorizontelescope.org/simulations-gallery.

33. Dokuchaev, V.I. To see invisible: image of the event horizon within the black hole shadow. *Intern. J. Mod. Phys. D* **2019**, *28*, 1941005; DOI: 10.1142/S0218271819410050.

34. Dokuchaev, V.I.; Nazarova, N.O. Event horizon image within black hole shadow. *J. Exp. Theor. Phys.* **2019**, *128*, 578–585; DOI: 10.1134/S1063776119030026.

35. Dokuchaev, V.I.; Nazarova, N.O.; Smirnov, V.P. Event horizon silhouette. *arXiv* **2019**, arXiv:1903.09594 [astro-ph.HE].

36. Boyer, R.H.; Lindquist, R. W. Maximal Analytic Extension of the Kerr Metric. *J. Math. Phys.* **1967**, *8*, 265–282; DOI: 10.1063/1.1705193.

37. Carter, B. Global Structure of the Kerr Family of Gravitational Fields. *Phys. Rev.* **1968**, *174*, 1559–1571; DOI: 10.1103/PhysRev.174.1559.

38. Cunningham, C.T.; Bardeen, J.M. The Optical Appearance of a Star Orbiting an Extreme Kerr Black Hole. *Astrophys. J.* **1973**, *183*, 237–264; DOI: 10.1086/152223.

39. Viergutz, S.U. Image generation in Kerr geometry. I. Analytical investigations on the stationary emitter-observer problem. *Astron. Astrophys.* **1993**, *272*, 355–377.

40. Rauch, K.P.; Blandford, R.D. Optical Caustics in a Kerr Spacetime and the Origin of Rapid X-Ray Variability in Active Galactic Nuclei. *Astrophys J.* **1994**, *421*, 46–68; DOI: 10.1086/173625.

41. Gralla, S.E.; Holz, D.E.; Wald, R.M. Black Hole Shadows, Photon Rings, and Lensing Rings. *arXiv* **2019**, arXiv:1906.00873. [astro-ph.HE].